Title

Molecular Langmuir—Blodgett Film for Silicon Anode Interface Engineering

Journal

ACS Applied Energy Materials, 5(9)

ISSN

2574-0962

Authors

Fang, Chen

Dopilka, Andrew

Gu, Yueran

et al.

Publication Date

2022-09-26

DOI

10.1021/acsaem.2c02130

ACS APPLIED ENERGY MATERIALS

www.acsaem.org Article

Molecular Langmuir–Blodgett Film for Silicon Anode Interface Engineering

Chen Fang, Andrew Dopilka, Yueran Gu, Vassilia Zorba, Robert Kostecki,* and Gao Liu*

Cite This: ACS Appl. Energy Mater. 2022, 5, 11655–11661 Read Online

ACCESS | Metrics & More | Article Recommendations

ABSTRACT: Silicon-based anodes are widely expected to vastly improve the performance of lithium-ion batteries (LIBs). However, the silicon anode interface is well-known to be unstable and reactive, leading to various electrolyte side reactions that would ultimately lower the battery performance. Consequently, it is critically important to rationally design the silicon anode to stabilize its interface. The Langmuir–Blodgett (LB) technique is a well-established, versatile, and powerful method for fabricating ultrathin films over solid substrates. Here, we utilize LB approach to generate thin films composed of small organic molecules over silicon electrodes as protective layers. Such molecular layers were found capable of mediating the electrochemical behavior of silicon electrodes in both aqueous and organic carbonate electrolytes. This study illustrates the applicability of small-molecule LB films in electrode interface engineering for LIB technology development.

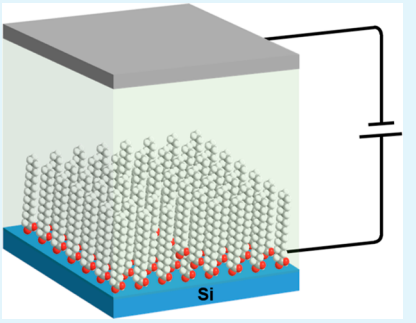

KEYWORDS: *lithium-ion battery, Langmuir–Blodgett technique, silicon electrode, solid electrolyte interphase, electrolyte reactions*

1. INTRODUCTION

Rechargeable batteries are pivotal for realizing vehicle electrification and large-scale green energy storage.[1−3] Despite the ubiquitous application of lithium-ion batteries (LIBs) in daily digital devices and in electric cars, the limited energy densities of contemporary LIBs pose outstanding obstacles for future evolution of battery-based portable electricity storage devices.[4−6] Consequently, substantial research efforts have been devoted to development of novel battery systems such as lithium–air batteries and lithium–sulfur batteries.[7−10] On the other hand, LIB is still an important player in the battery competition when silicon (Si) is employed, which is a low-cost anode material with a theoretically high capacity beyond 3500 mAh/g that is plausibly 10 times higher than that of graphite anodes.[11,12] Although principally favorable, Si anodes are confronted with a series of setbacks such as dramatic volume changes, high surface reactivity, and unstable solid electrolyte interphase (SEI) in charging and discharging processes.[13,14] Chemical developments of silicon anodes include binder engineering,[15,16] electrolyte optimization,[17−20] Si composite enhancement,[21−23] nanostructured Si anode,[24,25] and prelithiation.[26,27] It is also a common strategy to improve the SEI layers to minimize the adverse effects of Si lithiation/delithiation by electrolyte additives, which could electrochemically produce protective layers on electrode surfaces.[28−30] Additionally, functional artificial SEIs have been constructed with nonreactive thin films that are fabricated externally.[31] For example, graphene-based artificial SEIs have been applied to the $LiMn_2O_4$ cathode[32] and the lithium metal anode[33] to improve the performances of these electrodes. Such graphene thin films are constructed via Langmuir–Blodgett (LB) techniques.

LB technique is a classic strategy for creating monolayers and thin films with supramolecular structures, which are referred to as LB films. LB films are typically generated by organizing molecules or nanomaterials into a dense monolayer over a subphase (commonly water), followed by transferring the monolayer onto a flat substrate. Repeated deposition of monolayers leads to creation of multilayered thin films.[34,35] Compared to other thin-film techniques such as self-assembled monolayers,[36,37] where nanopatterns could be achieved spontaneously,[38,39] LB technique is often known to be technically more challenging and time-consuming. Nevertheless, LB technique depends on simple instrumentation that is readily compatible with various materials as well as large-area film fabrication, which are advantageous for industrial application.[40] The existing applications of LB techniques in battery technology include electrode fabrication, interlayer and artificial SEI construction, and electrochemical diagnosis.[31]

Anode SEIs in LIBs are typically composed of both inorganic and organic layers.[41,42] Rationally engineered organic layers on Si electrodes have attracted wide research attention in recent years, commonly utilizing surface functionalization of

Received: July 6, 2022
Accepted: August 24, 2022
Published: September 7, 2022

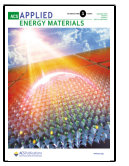

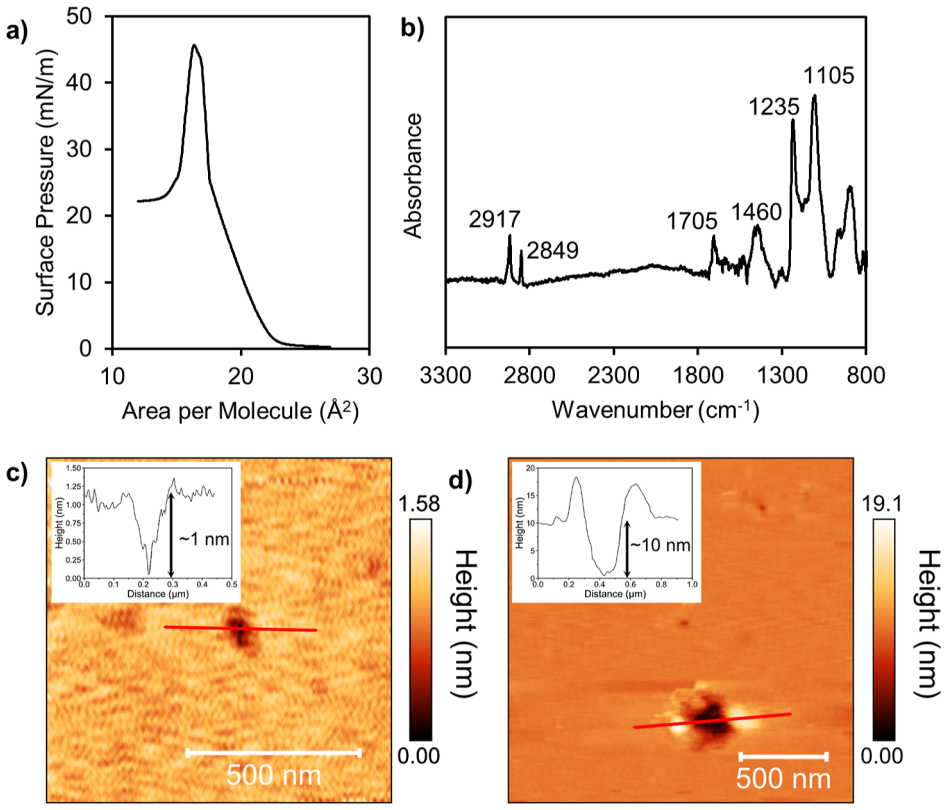

Figure 1. (a) Surface pressure−area (π−A) isotherm of SA monolayer at the air−water interface. (b) FTIR spectrum of the three-layer SA LB film on the silicon wafer. AFM images of (c) 1-layer and (d) 11-layer SA LB films on the silicon wafer (inserted images demonstrate the height profile across the defects).

Si materials via covalent chemical bonding.[43−48] Silicon surface decoration could also be achieved with non-covalently bonded layers, such as LB films.[49] In this work, we investigate the application of LB films for Si electrode SEI engineering. Specifically, we demonstrate that LB films of stearic acid (SA) molecules could be fabricated over the Si anode surface and that such organic LB films could be used to mediate the electrochemistry of Si wafers and Si thin-film electrodes.

2. MATERIALS AND METHODS

Stearic acid, sodium perchlorate, and copper(II) perchlorate were obtained from Sigma Aldrich. Water was obtained from a Milli-Q water purification system (Millipore). Organic solvents, copper sulfate, and sulfuric acid were obtained from VWR. Carbonate electrolyte was obtained from Tomiyama Pure Chemical Industries, LTD. Silicon wafer (n-doped, 0.002−0.005 Ω cm) was obtained from International Wafer Service, Inc and was cleaned with oxygen plasma (with G500 Plasma Cleaning System, Yield Engineering Systems). Metal-coating process was accomplished with a multitarget co-sputtering instrument, and Cu coating was sputtered over a thin Ti adhesion layer. Silicon thin-film electrodes were fabricated by sputtering Si thin films onto Cu-coated glass disks following reported protocols.[50−53] The obtained thin Si films were amorphous, and the thickness of the amorphous films was about 50 nm. There were thin oxide layers on the surface of Si thin films, and the samples were handled in air. It was found that the thin oxide layers did not significantly impact the electrochemical properties of the Si electrodes.

LB films were fabricated with a KSV NIMA LB trough (Biolin Scientific). The trough was thoroughly rinsed with ethanol and water before use. Stearic acid was predissolved in chloroform to produce a solution with 1 mg/mL concentration. The solution was spread over the water surface in the LB trough using a microsyringe. After evaporation of the solvent, the film was compressed at a barrier moving speed of 10 mm/min. The LB films were transferred onto silicon substrates by vertical dipping (5 mm/min) at a surface pressure of 28 mN/m. The multilayer LB films were fabricated in Y-type. For characterization of LB films, the surface morphology was measured by atomic force microscopy (AFM, Neaspec) in the constant tapping mode, and the images were taken with a tapping amplitude of 90−95 nm and a resolution of 19.5 nm/pixel. Fourier transform infrared (FTIR) spectroscopy was accomplished with a Nicolet iS50 spectrometer (Thermo Fisher).

Electrochemical measurements were carried out with a VSP300 potentiostat (Biologic Co.) and a PGSTAT302N potentiostat (AutoLab). For measurements in aqueous electrolyte, a small beaker cell (Figure 2a) was used with the Pt counter electrode and the Ag/AgCl (1 M KCl) reference electrode. The electrical connection to the silicon wafer was achieved with the copper wire attached at the back side of the wafer (coated with copper layer). The wafer was wrapped with epoxy resin to only expose the front side for electrochemical measurement. The aqueous electrolytes included 1 M KCl with 1 mM $K_3Fe(CN)_6$, 0.1 M $NaClO_4$ with 0−10 mM $Cu(ClO_4)_2$, and 1 M H_2SO_4 with 0.5 M $CuSO_4$. Cyclic voltammetry (CV) was carried out at a rate of 0.1 V/s for aqueous systems. For Cu electrodeposition reaction, Cu foil was used as the CE instead of Pt wire. For electrochemical measurements with the silicon thin-film electrode, the pouch cell was fabricated with the lithium foil counter electrode, a Celgard separator, and 1.2 M $LiPF_6$ ethylene carbonate/ethyl methyl carbonate (3:7 w/w) electrolyte. The cells were tested at 30 °C. CV measurements in carbonate electrolytes were carried out at a rate of 0.1 mV/s, and the voltage hold test was carried out at 50 mV versus Li/Li^+.

3. RESULTS AND DISCUSSION

The surface pressure−area (π−A) isotherm of the SA monolayer at the air−water interface is shown in Figure 1a.

https://doi.org/10.1021/acsaem.2c02130
ACS Appl. Energy Mater. 2022, 5, 11655−11661

The evolution of SA monolayer during compressing underwent a typical process successively consisting of the gaseous state, liquid state, solid state, and collapsed state (as area per molecule decreasing). The transition point between the liquid condensed state and the solid state, namely, the curve slope changing point in the compressed state, was observed at a surface pressure of 25 mN/m, which is consistent with previous reports.[54−56] SA monolayers were transferred onto the Si wafer via vertical dipping method, and FTIR spectrum of the thin films on the Si wafer is shown in Figure 1b. The peak at 1705 cm^{-1} is ascribed to carbonyl stretching, and the peaks at 2917, 2849, and 1460 cm^{-1} are attributed to CH_2 groups.[57−59] The large background peaks at 1235 and 1105 cm^{-1} originated from the oxide species at the silicon wafer surface.[60] AFM images of SA films on silicon wafers with 1-layer and 11-layer thicknesses (Figure 1c,d) demonstrate that the films have a flat and smooth morphology. The height profile across defect regions could be utilized to illustrate the film thickness.[61] The defect depths of 1-layer and 11-layer SA films were found to be about 1 and 10 nm, respectively, the contrast between which is in good agreement with their layer number difference. With the isotherm, FTIR and AFM characterizations, it is confirmed that single- and multi-layer SA LB films were successfully fabricated on silicon wafer substrates.

After verification of LB film transfer onto the Si wafer, the electrochemical impact of the LB film was firstly examined in aqueous electrolyte. The electrochemical cell setup is shown in Figure 2a, where the Si wafer working electrode (WE), the Pt

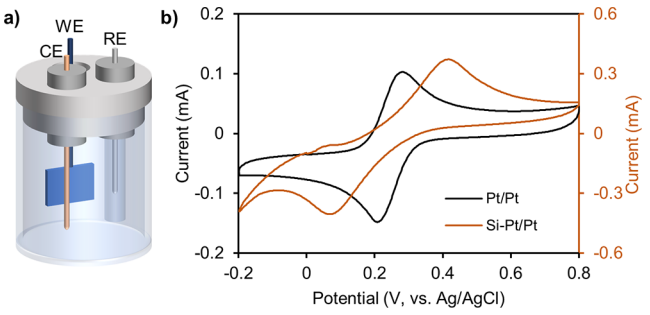

Figure 2. (a) Schematic illustration of the beaker cell with WE, CE, and RE. (b) CV measurements in $K_3Fe(CN)_6$ solution between two Pt electrodes (black) and between Pt-coated Si wafer WE and Pt CE (yellow).

wire counter electrode (CE), and the Ag/AgCl reference electrode (RE) are positioned in close proximity. The suitability of this cell setup was investigated by CV measurement of $K_3Fe(CN)_6$ solution. For the initial test, the Si WE was replaced by a Pt WE, same as the CE. As shown in Figure 2b (black curve), the potential separation between the cathodic and anodic peaks is 74 mV, which is close to a reversible reaction,[62,63] demonstrating that the cell setup was appropriate. Next, a Pt-coated Si wafer WE was paired with a Pt CE to carry out the identical experiment, and the result is shown in Figure 2b (yellow curve). The potential difference between the two peaks increased appreciably to 346 mV. Such a result illustrates the imperfection of the semiconducting Si wafer as the WE in aqueous electrolyte.[64]

To reliably explore the impacts of LB films on the electrochemical behaviors of the Si wafer, Cu electrodeposition reaction was selected as the testing platform. The Si wafer electrode was found to be electrochemically nonactive in the $NaClO_4$ supporting electrolyte between −0.7 and 0.3 V versus Ag/AgCl (Figure 3a), resolving the concern of Si wafer-induced side reactions. When 1 mM $Cu(ClO_4)_2$ was added to the $NaClO_4$ supporting electrolyte, it was found that such a low Cu concentration was not sufficient to result in noticeable Cu electrodeposition (Figure 3b, dashed curve). Increasing $Cu(ClO_4)_2$ concentration to 10 mM successfully led to unambiguous observation of Cu deposition on the Si wafer electrode between −0.05 and −0.7 V versus Ag/AgCl. At a more negative potential, the Cu deposition signal is overlapped with that from hydrogen evolution. Thus, the influence of the SA LB film was subsequently probed with 10 mM $Cu(ClO_4)_2$ electrolyte above the potential of −0.7 V versus Ag/AgCl. As shown in Figure 3c, the bare Si wafer electrode showed clear Cu electrodeposition between −0.05 and −0.7 V versus Ag/AgCl, while the SA LB film could significantly suppress the Cu reduction reaction at the Si wafer surface, as evidenced by the reduced current. Separately, Cu deposition was also examined with $CuSO_4$ as the copper salt in H_2SO_4 electrolyte. As shown in Figure 3d, the Si wafer electrode was nonactive in sulfuric acid electrolyte between −1.1 and 0.8 V, and minor hydrogen evolution occurred beyond −1.1 V. Addition of $CuSO_4$ in the electrolyte resulted in Cu deposition starting at about −0.1 V, and a very broad peak corresponding to Cu reduction was observed. In comparison, the existence of SA LB films could suppress Cu reduction. These observations demonstrate that LB films could mediate electrochemical reactions at the Si wafer electrode interface.[65]

To further explore the applicability of the LB film in LIBs under an organic carbonate electrolyte environment, Si thin-film electrodes were fabricated to be examined in an LIB pouch cell setup (versus lithium foil CE). The Si thin-film electrode would not undergo significant mechanical degradation during cycling, which makes the Si thin film a good platform for investigating the chemical effects of LB films on electrode's reactions. Figure 4a demonstrates the first-cycle CV measurement of the cells starting from open-circuit voltage (OCV). The SEI formation was observed at 0.39 V versus Li/Li^+, and the presence of five layers of SA LB films appreciably suppressed the SEI formation. As shown in Figure 4b,c, the SEI reactions in later cycles were not outstanding. At 50 mV versus Li/Li^+, the lithiation capacities of the Si thin-film electrodes with and without the SA film are 89 and 87 μA h/cm^2, respectively, for the first cycle. The values for the second cycle are 54 and 57 μA h/cm^2, respectively. These results demonstrate that the introduction of the LB film did not disturb the Si lithiation and delithiation reactions. During the repeated CV cycling, the lithiation/delithiation processes seem slightly suppressed with the presence of LB films, which was likely due to the limiting effect of LB films on the charge and mass transfer across the silicon interface.

Potentiostatic hold is an accelerated technique for estimating the calendar life of LIBs,[66,67] and the cycled cells were then subjected to potentiostatic hold at 50 mV versus Li/Li^+. After a period of 12 h, the parasitic current was found smaller for the Si thin-film electrode covered with the five-layer SA LB film (Figure 4d), which indicates potentially a longer calendar life. Such an observation is consistent with the CV measurement, where LB films were found to suppress electrolyte side reactions. These findings indicate that LB films could also serve to tune the surface properties of the Si electrode in organic carbonate electrolytes and thus to mediate the reactions at the

https://doi.org/10.1021/acsaem.2c02130
ACS Appl. Energy Mater. 2022, 5, 11655−11661

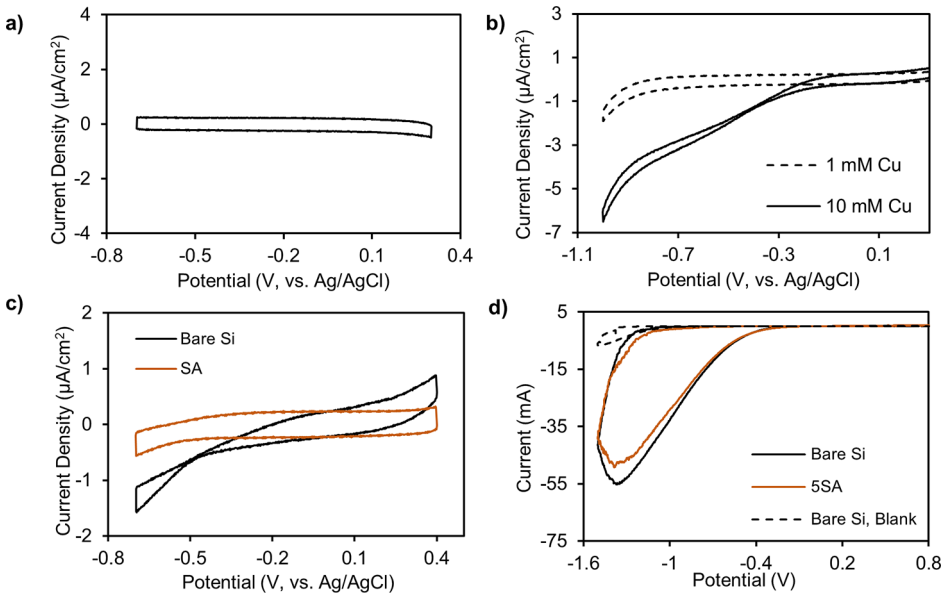

Figure 3. CV measurements of the Si wafer electrode in (a) 0.1 M $NaClO_4$ electrolyte and (b) 0.1 M $NaClO_4$ electrolyte with $Cu(ClO_4)_2$. (c) CV measurements of Si wafer electrodes with (yellow) and without (black) the SA LB film in 10 mM $Cu(ClO_4)_2$ electrolyte (0.1 M $NaClO_4$). (d) CV measurements of Si wafer electrodes with (yellow) and without (black) the five-layer SA LB film in 0.5 M $CuSO_4$ electrolyte (1 M H_2SO_4) and bare Si wafer in $CuSO_4$-blank electrolyte (dashed).

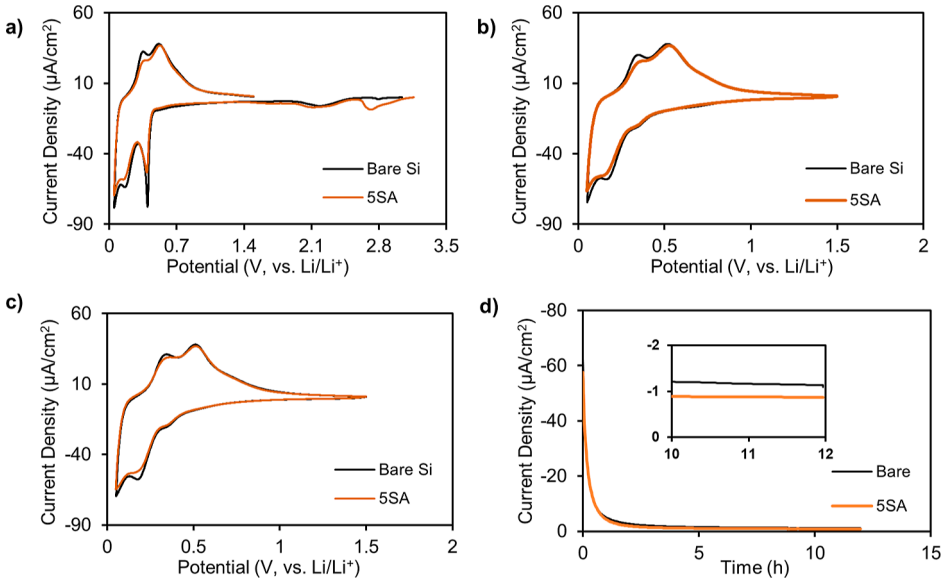

Figure 4. CV measurements of Si thin-film electrodes with and without SA LB film: (a) First cycle from OCV, (b) second cycle, and (c) fifth cycle. (d) Parasitic currents measured during 12 h potentiostatic hold at 50 mV versus Li/Li^+ (inserted image demonstrates the profile during 10−12 h).

Si electrode surface in LIBs. In practical Si electrodes, the Si particles would experience significant mechanical strains and surface condition changes. Multilayer films composed of small organic molecules, such as LB films, could serve as a reservoir of protective agents, where the organic molecules could possibly adapt to the expansion and shrinking of Si interfaces in a dynamic manner. Therefore, the LB films could serve as a platform for investigating artificial organic interfaces on Si electrode surfaces for improving the calendar life of Si-based batteries.

4. CONCLUSIONS

In summary, we have investigated the impact of small-molecule LB films on the electrochemical behavior of Si electrodes. Single- and multi-layer SA LB films have been fabricated at the air−water interface and transferred onto Si substrates, and these layers presented a flat and smooth morphology. In aqueous electrolyte, the SA LB film was found to suppress copper deposition on the Si wafer electrode, demonstrating the capability of small-molecule LB films in mediating Si electrode's behavior. Furthermore, the effect of LB films in LIBs with organic carbonate electrolyte was also examined. When cycled against lithium foil counter electrode, the Si thin-film electrode bearing SA LB films presented lower charge consumption in SEI formation. During the potentiostatic hold test, the LB films also led to a smaller terminal parasitic current. These results indicate that LB films composed of small organic molecules can protect the Si electrode from side

https://doi.org/10.1021/acsaem.2c02130
ACS Appl. Energy Mater. 2022, 5, 11655−11661

reactions at the electrode/electrolyte interface such as extensive electrolyte decomposition. As the structure and functionality of the LB films could be readily tuned by choosing different organic molecules or molecule combinations, the molecular LB film strategy is expected to provide a facile and versatile platform for interface engineering of Si electrode in LIBs.

AUTHOR INFORMATION

Corresponding Authors

Robert Kostecki − *Energy Storage and Distributed Resources Division, Lawrence Berkeley National Laboratory, Berkeley, California 94720, United States*; Email: r_kostecki@lbl.gov

Gao Liu − *Energy Storage and Distributed Resources Division, Lawrence Berkeley National Laboratory, Berkeley, California 94720, United States*; orcid.org/0000-0001-6886-0507; Email: gliu@lbl.gov

Authors

Chen Fang − *Energy Storage and Distributed Resources Division, Lawrence Berkeley National Laboratory, Berkeley, California 94720, United States*; orcid.org/0000-0003-2101-1991

Andrew Dopilka − *Energy Storage and Distributed Resources Division, Lawrence Berkeley National Laboratory, Berkeley, California 94720, United States*

Yueran Gu − *Energy Storage and Distributed Resources Division, Lawrence Berkeley National Laboratory, Berkeley, California 94720, United States; Department of Mechanical Engineering, University of California Berkeley, Berkeley, California 94720, United States*

Vassilia Zorba − *Energy Storage and Distributed Resources Division, Lawrence Berkeley National Laboratory, Berkeley, California 94720, United States; Department of Mechanical Engineering, University of California Berkeley, Berkeley, California 94720, United States*

Complete contact information is available at: https://pubs.acs.org/10.1021/acsaem.2c02130

Notes

The authors declare no competing financial interest.

ACKNOWLEDGMENTS

This research was funded by the Assistant Secretary for Energy Efficiency, Vehicle Technologies Office of the U.S. Department of Energy, under the Si Consortium Program. Fourier transform infrared spectroscopy was performed at the Molecular Foundry at Lawrence Berkeley National Laboratory. Work at the Molecular Foundry was supported by the Office of Science, Office of Basic Energy Sciences, of the U.S. Department of Energy under contract No. DE-AC02-05CH11231.

REFERENCES

(1) Moon, J.; Lee, H. C.; Jung, H.; Wakita, S.; Cho, S.; Yoon, J.; Lee, J.; Ueda, A.; Choi, B.; Lee, S.; Ito, K.; Kubo, Y.; Lim, A. C.; Seo, J. G.; Yoo, J.; Lee, S.; Ham, Y.; Baek, W.; Ryu, Y.-G.; Han, I. T. Interplay between electrochemical reactions and mechanical responses in silicon−graphite anodes and its impact on degradation. *Nat. Commun.* **2021**, *12*, 2714.

(2) Liu, Z.; He, X.; Fang, C.; Camacho-Forero, L. E.; Zhao, Y.; Fu, Y.; Feng, J.; Kostecki, R.; Balbuena, P. B.; Zhang, J.; Lei, J.; Liu, G. Reversible Crosslinked Polymer Binder for Recyclable Lithium Sulfur Batteries with High Performance. *Adv. Funct. Mater.* **2020**, *30*, 2003605.

(3) Zhao, Y.; Fang, C.; Zhang, G.; Hubble, D.; Nallapaneni, A.; Zhu, C.; Zhao, Z.; Liu, Z.; Lau, J.; Fu, Y.; Liu, G. A Micelle Electrolyte Enabled by Fluorinated Ether Additives for Polysulfide Suppression and Li Metal Stabilization in Li-S Battery. *Front. Chem.* **2020**, *8*, 484.

(4) Eshetu, G. G.; Zhang, H.; Judez, X.; Adenusi, H.; Armand, M.; Passerini, S.; Figgemeier, E. Production of high-energy Li-ion batteries comprising silicon-containing anodes and insertion-type cathodes. *Nat. Commun.* **2021**, *12*, 5459.

(5) Fang, C.; Xiao, H.; Zheng, T.; Bai, H.; Liu, G. Organic Solvent Free Process to Fabricate High Performance Silicon/Graphite Composite Anode. *J. Compos. Sci.* **2021**, *5*, 188.

(6) Zhou, S.; Fang, C.; Song, X.; Liu, G. The Influence of Compact and Ordered Carbon Coating on Solid-state Behaviors of Silicon during Electrochemical Processes. *Carbon Energy* **2020**, *2*, 143−150.

(7) Chen, K.; Yang, D.-Y.; Huang, G.; Zhang, X.-B. Lithium−Air Batteries: Air-Electrochemistry and Anode Stabilization. *Acc. Chem. Res.* **2021**, *54*, 632−641.

(8) Guo, Z.; Zhang, Q.; Wang, C.; Zhang, Y.; Dong, S.; Cui, G. I-containing Polymer/Alloy Layer-Based Li Anode Mediating High-Performance Lithium−Air Batteries. *Adv. Funct. Mater.* **2022**, *32*, 2108993.

(9) Li, Z.; Fang, C.; Qian, C.; Zhou, S.; Song, X.; Ling, M.; Liang, C.; Liu, G. Polyisoprene Captured Sulfur Nanocomposite Materials for High-Areal-Capacity Lithium Sulfur Battery. *ACS Appl. Polym. Mater.* **2019**, *1*, 1965−1970.

(10) Fang, C.; Zhang, G.; Lau, J.; Liu, G. Recent Advances in Polysulfide Mediation of Lithium-sulfur Batteries via Facile Cathode and Electrolyte Modification. *APL Mater.* **2019**, *7*, 080902.

(11) Lee, H. A.; Shin, M.; Kim, J.; Choi, J. W.; Lee, H. Designing Adaptive Binders for Microenvironment Settings of Silicon Anode Particles. *Adv. Mater.* **2021**, *33*, 2007460.

(12) Xiao, H.; Fang, C.; Zheng, T.; Bai, H.; Liu, G. Investigation of SiOx anode fading mechanism with limited capacity cycling. *APL Mater.* **2022**, *10*, 011108.

(13) Han, B.; Zhang, Y.; Liao, C.; Trask, S. E.; Li, X.; Uppuluri, R.; Vaughey, J. T.; Key, B.; Dogan, F. Probing the Reactivity of the Active Material of a Li-Ion Silicon Anode with Common Battery Solvents. *ACS Appl. Mater. Interfaces* **2021**, *13*, 28017−28026.

(14) Zhang, C.; Wang, F.; Han, J.; Bai, S.; Tan, J.; Liu, J.; Li, F. Challenges and Recent Progress on Silicon-Based Anode Materials for Next-Generation Lithium-Ion Batteries. *Small Struct.* **2021**, *2*, 2100009.

(15) Wang, X.; Liu, S.; Zhang, Y.; Wang, H.; Aboalhassan, A. A.; Li, G.; Xu, G.; Xue, C.; Yu, J.; Yan, J.; Ding, B. Highly Elastic Block Copolymer Binders for Silicon Anodes in Lithium-Ion Batteries. *ACS Appl. Mater. Interfaces* **2020**, *12*, 38132−38139.

(16) Liu, Z.; Fang, C.; He, X.; Zhao, Y.; Xu, H.; Lei, J.; Liu, G. In Situ-Formed Novel Elastic Network Binder for a Silicon Anode in Lithium-Ion Batteries. *ACS Appl. Mater. Interfaces* **2021**, *13*, 46518−46525.

(17) Xu, Z.; Yang, J.; Li, H.; Nuli, Y.; Wang, J. Electrolytes for advanced lithium ion batteries using silicon-based anodes. *J. Mater. Chem. A* **2019**, *7*, 9432−9446.

(18) Hopkins, E.; Frisco, S.; Pekarek, R.; Stetson, C.; Huey, Z.; Harvey, S.; Li, X.; Key, B.; Fang, C.; Liu, G.; Yang, G.; Teeter, G.; Neale, N.; Veith, G. Examining CO_2 as an Additive for Solid Electrolyte Interphase Formation on Silicon Anodes. *J. Electrochem. Soc.* **2021**, *168*, 030534.

(19) Han, B.; Liao, C.; Dogan, F.; Trask, S. E.; Lapidus, S. H.; Vaughey, J. T.; Key, B. Using Mixed Salt Electrolytes to Stabilize Silicon Anodes for Lithium-Ion Batteries via in Situ Formation of Li−M−Si Ternaries (M = Mg, Zn, Al, Ca). *ACS Appl. Mater. Interfaces* **2019**, *11*, 29780−29790.

(20) Hubble, D.; Brown, D. E.; Zhao, Y.; Fang, C.; Lau, J.; McCloskey, B. D.; Liu, G. Liquid electrolyte development for low-temperature lithium-ion batteries. *Energy Environ. Sci.* **2022**, *15*, 550−578.

(21) Casino, S.; Niehoff, P.; Börner, M.; Winter, M. Protective coatings on silicon particles and their effect on energy density and specific energy in lithium ion battery cells: A model study. *J. Energy Storage* **2020**, *29*, 101376.
(22) Zhou, S.; Fang, C.; Song, X.; Liu, G. Highly Ordered Carbon Coating Prepared with Polyvinylidene Chloride Precursor for High-Performance Silicon Anodes in Lithium-Ion Batteries. *Batteries Supercaps* **2021**, *4*, 240−247.
(23) Wang, F.; Song, C.; Zhao, B.; Sun, L.; Du, H. One-pot solution synthesis of carbon-coated silicon nanoparticles as an anode material for lithium-ion batteries. *Chem. Commun.* **2020**, *56*, 1109−1112.
(24) Li, Y.; Yan, K.; Lee, H.-W.; Lu, Z.; Liu, N.; Cui, Y. Growth of conformal graphene cages on micrometre-sized silicon particles as stable battery anodes. *Nat. Energy* **2016**, *1*, 15029.
(25) Jiang, B.; Zeng, S.; Wang, H.; Liu, D.; Qian, J.; Cao, Y.; Yang, H.; Ai, X. Dual Core−Shell Structured Si@SiOx@C Nanocomposite Synthesized via a One-Step Pyrolysis Method as a Highly Stable Anode Material for Lithium-Ion Batteries. *ACS Appl. Mater. Interfaces* **2016**, *8*, 31611−31616.
(26) Zhao, J.; Lu, Z.; Liu, N.; Lee, H.-W.; McDowell, M. T.; Cui, Y. Dry-air-stable lithium silicide−lithium oxide core−shell nanoparticles as high-capacity prelithiation reagents. *Nat. Commun.* **2014**, *5*, 5088.
(27) Zhu, T.; Tran, T.-N.; Fang, C.; Liu, D.; Herle, S. P.; Guan, J.; Gopal, G.; Joshi, A.; Cushing, J.; Minor, A. M.; Liu, G. Lithium substituted poly(amic acid) as a water-soluble anode binder for high-temperature pre-lithiation. *J. Power Sources* **2022**, *521*, 230889.
(28) Kim, J.; Chae, O. B.; Lucht, B. L. Perspective—Structure and Stability of the Solid Electrolyte Interphase on Silicon Anodes of Lithium-ion Batteries. *J. Electrochem. Soc.* **2021**, *168*, 030521.
(29) Fang, C.; Lau, J.; Hubble, D.; Khomein, P.; Dailing, E. A.; Liu, Y.; Liu, G. Large-Molecule Decomposition Products of Electrolytes and Additives Revealed by On-Electrode Chromatography and MALDI. *Joule* **2021**, *5*, 415−428.
(30) Fang, C.; Tran, T.-N.; Zhao, Y.; Liu, G. Electrolyte decomposition and solid electrolyte interphase revealed by mass spectrometry. *Electrochim. Acta* **2021**, *399*, 139362.
(31) Fang, C.; Yoon, I.; Hubble, D.; Tran, T.-N.; Kostecki, R.; Liu, G. Recent Applications of Langmuir−Blodgett Technique in Battery Research. *ACS Appl. Mater. Interfaces* **2022**, *14*, 2431−2439.
(32) Zhi, J.; Yazdi, A. Z.; Valappil, G.; Haime, J.; Chen, P. Artificial Solid Electrolyte Interphase for Aqueous Lithium Energy Storage Systems. *Sci. Adv.* **2017**, *3*, No. e1701010.
(33) Kim, M. S.; Ryu, J.-H.; Deepika; Lim, Y. R.; Nah, I. W.; Lee, K.-R.; Archer, L. A.; Il Cho, W. Langmuir−Blodgett artificial solid-electrolyte interphases for practical lithium metal batteries. *Nat. Energy* **2018**, *3*, 889−898.
(34) McCullough, D. H., III; Regen, S. L. Don't Forget Langmuir−Blodgett Films. *Chem. Commun.* **2004**, *24*, 2787−2791.
(35) Hussain, S. A.; Dey, B.; Bhattacharjee, D.; Mehta, N. Unique supramolecular assembly through Langmuir − Blodgett (LB) technique. *Heliyon* **2018**, *4*, No. e01038.
(36) Gooding, J. J.; Ciampi, S. The molecular level modification of surfaces: from self-assembled monolayers to complex molecular assemblies. *Chem. Soc. Rev.* **2011**, *40*, 2704−2718.
(37) He, J.; Fang, C.; Shelp, R. A.; Zimmt, M. B. Tracking Invisible Transformations of Physisorbed Monolayers: LDI-TOF and MALDI-TOF Mass Spectrometry as Complements to STM Imaging. *Langmuir* **2017**, *33*, 459−467.
(38) Velpula, G.; Takeda, T.; Adisoejoso, J.; Inukai, K.; Tahara, K.; Mali, K. S.; Tobe, Y.; De Feyter, S. On the formation of concentric 2D multicomponent assemblies at the solution−solid interface. *Chem. Commun.* **2017**, *53*, 1108−1111.
(39) Fang, C.; Zhu, H.; Chen, O.; Zimmt, M. B. Reactive Two-component Monolayers Template Bottom-up Assembly of Nanoparticle Arrays on HOPG. *Chem. Commun.* **2018**, *54*, 8056−8059.
(40) Ariga, K. Don't Forget Langmuir−Blodgett Films 2020: Interfacial Nanoarchitectonics with Molecules, Materials, and Living Objects. *Langmuir* **2020**, *36*, 7158−7180.
(41) Heiskanen, S. K.; Kim, J.; Lucht, B. L. Generation and Evolution of the Solid Electrolyte Interphase of Lithium-Ion Batteries. *Joule* **2019**, *3*, 2322−2333.
(42) Zhou, Y.; Su, M.; Yu, X.; Zhang, Y.; Wang, J.-G.; Ren, X.; Cao, R.; Xu, W.; Baer, D. R.; Du, Y.; Borodin, O.; Wang, Y.; Wang, X.-L.; Xu, K.; Xu, Z.; Wang, C.; Zhu, Z. Real-time mass spectrometric characterization of the solid−electrolyte interphase of a lithium-ion battery. *Nat. Nanotechnol.* **2020**, *15*, 224−230.
(43) Jiang, S.; Yang, Z.; Liu, Y.; Johnson, N.; Bloom, I.; Zhang, L.; Zhang, Z. Engineering the Si Anode Interface via Particle Surface Modification: Embedded Organic Carbonates Lead to Enhanced Performance. *ACS Appl. Energy Mater.* **2021**, *4*, 8193−8200.
(44) Qian, C.; Zhao, J.; Sun, Y.; Lee, H. R.; Luo, L.; Makaremi, M.; Mukherjee, S.; Wang, J.; Zu, C.; Xia, M.; Wang, C.; Singh, C. V.; Cui, Y.; Ozin, G. A. Electrolyte-Phobic Surface for the Next-Generation Nanostructured Battery Electrodes. *Nano Lett.* **2020**, *20*, 7455−7462.
(45) Schulze, M. C.; Carroll, G. M.; Martin, T. R.; Sanchez-Rivera, K.; Urias, F.; Neale, N. R. Hydrophobic versus Hydrophilic Interfacial Coatings on Silicon Nanoparticles Teach Us How to Design the Solid Electrolyte Interphase in Silicon-Based Li-Ion Battery Anodes. *ACS Appl. Energy Mater.* **2021**, *4*, 1628−1636.
(46) Jiang, S.; Hu, B.; Sahore, R.; Zhang, L.; Liu, H.; Zhang, L.; Lu, W.; Zhao, B.; Zhang, Z. Surface-Functionalized Silicon Nanoparticles as Anode Material for Lithium-Ion Battery. *ACS Appl. Mater. Interfaces* **2018**, *10*, 44924−44931.
(47) Tan, T.; Lee, P.-K.; Zettsu, N.; Teshima, K.; Yu, D. Y. W. Highly stable lithium-ion battery anode with polyimide coating anchored onto micron-size silicon monoxide via self-assembled monolayer. *J. Power Sources* **2020**, *453*, 227874.
(48) Kang, S.; Yang, K.; White, S. R.; Sottos, N. R. Silicon Composite Electrodes with Dynamic Ionic Bonding. *Adv. Energy Mater.* **2017**, *7*, 1700045.
(49) Ariga, K.; Yamauchi, Y.; Mori, T.; Hill, J. P. 25th Anniversary Article: What Can Be Done with the Langmuir-Blodgett Method? Recent Developments and its Critical Role in Materials Science. *Adv. Mater.* **2013**, *25*, 6477−6512.
(50) Lee, S.-J.; Lee, J.-K.; Chung, S.-H.; Lee, H.-Y.; Lee, S.-M.; Baik, H.-K. Stress effect on cycle properties of the silicon thin-film anode. *J. Power Sources* **2001**, *97*−*98*, 191−193.
(51) Maranchi, J. P.; Hepp, A. F.; Kumta, P. N. High Capacity, Reversible Silicon Thin-Film Anodes for Lithium-Ion Batteries. *Electrochem. Solid-State Lett.* **2003**, *6*, A198.
(52) Lee, K.-L.; Jung, J.-Y.; Lee, S.-W.; Moon, H.-S.; Park, J.-W. Electrochemical characteristics of a-Si thin film anode for Li-ion rechargeable batteries. *J. Power Sources* **2004**, *129*, 270−274.
(53) Márquez, E.; Saugar, E.; Díaz, J. M.; García-Vázquez, C.; Fernández-Ruano, S. M.; Blanco, E.; Ruiz-Pérez, J. J.; Minkov, D. A. The influence of Ar pressure on the structure and optical properties of non-hydrogenated a-Si thin films grown by rf magnetron sputtering onto room-temperature glass substrates. *J. Non-Cryst. Solids* **2019**, *517*, 32−43.
(54) Parra-Barraza, H.; Burboa, M. G.; Sánchez-Vázquez, M.; Juárez, J.; Goycoolea, F. M.; Valdez, M. A. Chitosan−Cholesterol and Chitosan−Stearic Acid Interactions at the Air−Water Interface. *Biomacromolecules* **2005**, *6*, 2416−2426.
(55) Ahmed, I.; Haque, A.; Bhattacharyya, S.; Patra, P.; Plaisier, J. R.; Perissinotto, F.; Bal, J. K. Vitamin C/Stearic Acid Hybrid Monolayer Adsorption at Air−Water and Air−Solid Interfaces. *ACS Omega* **2018**, *3*, 15789−15798.
(56) Sakai, A.; Wang, S. H.; Péres, L. O.; Caseli, L. Controlling the luminescence properties of poly(p-phenylene vinylene) entrapped in Langmuir and Langmuir−Blodgett films of stearic acid. *Synth. Met.* **2011**, *161*, 1753−1759.
(57) Kimura, F.; Umemura, J.; Takenaka, T. FTIR-ATR studies on Langmuir-Blodgett films of stearic acid with 1-9 monolayers. *Langmuir* **1986**, *2*, 96−101.
(58) Mukherjee, S.; Datta, A.; Giglia, A.; Mahne, N.; Nannarone, S. Relating structure with morphology: A comparative study of perfect Langmuir−Blodgett multilayers. *Chem. Phys. Lett.* **2008**, *451*, 80−87.

https://doi.org/10.1021/acsaem.2c02130
ACS Appl. Energy Mater. 2022, 5, 11655−11661

(59) Fang, C.; Liu, Z.; Lau, J.; Elzouka, M.; Zhang, G.; Khomein, P.; Lubner, S.; Ross, P. N.; Liu, G. Gradient Polarity Solvent Wash for Separation and Analysis of Electrolyte Decomposition Products on Electrode Surfaces. *J. Electrochem. Soc.* **2020**, *167*, 020506.
(60) Kopani, M.; Mikula, M.; Takahashi, M.; Rusnák, J.; Pinčík, E. FT IR spectroscopy of silicon oxide layers prepared with perchloric acid. *Appl. Surf. Sci.* **2013**, *269*, 106−109.
(61) Gupta, R. K.; Suresh, K. A. AFM studies on Langmuir-Blodgett films of cholesterol. *Eur. Phys. J. E: Soft Matter Biol. Phys.* **2004**, *14*, 35−42.
(62) Patel, A. N.; Collignon, M. G.; O'Connell, M. A.; Hung, W. O. Y.; McKelvey, K.; Macpherson, J. V.; Unwin, P. R. A New View of Electrochemistry at Highly Oriented Pyrolytic Graphite. *J. Am. Chem. Soc.* **2012**, *134*, 20117−20130.
(63) Fischer, L. M.; Tenje, M.; Heiskanen, A. R.; Masuda, N.; Castillo, J.; Bentien, A.; Émneus, J.; Jakobsen, M. H.; Boisen, A. Gold cleaning methods for electrochemical detection applications. *Microelectron. Eng.* **2009**, *86*, 1282−1285.
(64) Barrelet, C. J.; Robinson, D. B.; Cheng, J.; Hunt, T. P.; Quate, C. F.; Chidsey, C. E. D. Surface Characterization and Electrochemical Properties of Alkyl, Fluorinated Alkyl, and Alkoxy Monolayers on Silicon. *Langmuir* **2001**, *17*, 3460−3465.
(65) Arrington, D.; Curry, M.; Street, S.; Pattanaik, G.; Zangari, G. Copper electrodeposition onto the dendrimer-modified native oxide of silicon substrates. *Electrochim. Acta* **2008**, *53*, 2644−2649.
(66) McBrayer, J. D.; Rodrigues, M.-T. F.; Schulze, M. C.; Abraham, D. P.; Apblett, C. A.; Bloom, I.; Carroll, G. M.; Colclasure, A. M.; Fang, C.; Harrison, K. L.; Liu, G.; Minteer, S. D.; Neale, N. R.; Veith, G. M.; Johnson, C. S.; Vaughey, J. T.; Burrell, A. K.; Cunningham, B. Calendar aging of silicon-containing batteries. *Nat. Energy* **2021**, *6*, 866−872.
(67) Schulze, M. C.; Rodrigues, M.-T. F.; McBrayer, J. D.; Abraham, D. P.; Apblett, C. A.; Bloom, I.; Chen, Z.; Colclasure, A. M.; Dunlop, A. R.; Fang, C.; Harrison, K. L.; Liu, G.; Minteer, S. D.; Neale, N. R.; Robertson, D.; Tornheim, A. P.; Trask, S. E.; Veith, G. M.; Verma, A.; Yang, Z.; Johnson, C. Critical Evaluation of Potentiostatic Holds as Accelerated Predictors of Capacity Fade during Calendar Aging. *J. Electrochem. Soc.* **2022**, *169*, 050531.

https://doi.org/10.1021/acsaem.2c02130
ACS Appl. Energy Mater. 2022, 5, 11655−11661